INAF/OATs
LFI Project System Team

Planck LFI

TITLE: **ZLE Maps for the Planck Mission II: Simulated Flight Maps**

DOC. TYPE: Technical Note
PROJECT REF.: PL-LFI-OAT-TN-071 PAGE: 1 of 22
ISSUE/REV.: 1.0 DATE: January 31, 2011

Prepared by	Michele Maris	January 31, 2011
Agreed by	M. Bersanelli LFI Instrument Scientist C.R. Butler LFI Program Manager	
Approved by	N. Mandolesi LFI Principal Investigator	

CHANGE RECORD

Issue	Date	Sheet	Description of change	Release
0.0	20th Jan, 2011	All	First draft of document, number to be assigned	0.0
0.1	28th Jan, 2011	All	added figures,	0.1
0.5	31th Jan, 2011	All	number 071 assigned	0.5
1.0	31th Jan, 2011	All	First issue of the document	1.0

DISTRIBUTION LIST

Recipient	Company/Institute	E-mail address	Sent
Carlo Burigana	INAF/IASF-BO	burigana@iasfbo.inaf.it	January 31, 2011
Antony John Banday	MPA-Garching	banday@MPA-Garching.MPG.DE	January 31, 2011
Martin Reinecke	MPA-Garching	martin@MPA-Garching.MPG.DE	January 31, 2011
Tess Jaffe	CESR	tess.jaffe@cesr.fr	January 31, 2011
Andrea Zacchei	INAF-OATS	zacchei@oats.inaf.it	January 31, 2011
Fabio Finelli	INAF/IASF-BO	finelli@iasfbo.inaf.it	January 31, 2011
Alessandro Gruppuso	INAF/IASF-BO	gruppuso@iasfbo.inaf.it	January 31, 2011
Xi Chen	IPAC-Caltech	xchen@ipac.caltech.edu	January 31, 2011
Jose M. Diego	IFCA	jdiego@ifca.unican.es	January 31, 2011
Cecille Renault	IN	rcecile@in2p3.fr	January 31, 2011
Brendan Crill	JPL	Brendan.P.Crill@jpl.nasa.gov	January 31, 2011
Andrea Zonca	UCSB	zonca@deepspace.ucsb.edu	January 31, 2011

Contents

LIST OF ABBREVIATIONS

acronym	**Explanation**
LFI	Low Frequency Instrument
HFI	High Frequency Instrument
IDPs	Interplanetary Dust Particles
MOB	Mobile Object
SSB	Solar System Baricenter
SSO	Solar System Object
TBC	To Be Confirmed
TBD	To Be Defined
TOD	Time Ordered Data
TODs	Plural of TOD
TOI	Time Ordered Information
TODs	Plural of TOI
ZLE	Zodiacal Light Emission

1 Applicable and Reference Documents

Applicable Documents

[AD-1] Maris M., Burigana C., Fogliani S.,2005 *Simulation aspects on the zle modelling in the Planck mission* Internal Report IASF-BO 429/2005

[AD-2] Maris, M., 2001, PLANCK/*LFI - FS_ZOD: A Simulator of the Zodiacal Light Emission for the* PLANCK *Mission*, 2001, Planck/LFI Int.Rep.: PL-LFI-OAT-TN-023, Issue 1.0

[AD-3] Maris, M., Fogliani, S., Burigana, C., 2004, *How to use the Zodiacal Light Emission Maps for* PLANCK , Planck/LFI Int.Rep.: PL-LFI-OAT-TN-031, Issue 1.0, 2004, Dec 31th

[AD-4] *Maps of ZLE Contribution for the* PLANCK *Mission* Maris M., Burigana C., Fogliani S., 2004 Dec 31st, PL-LFI-OAT-TN-032

[AD-5] *ZLE: Spectral Dependence and K correction* Maris M., Burigana C., Fogliani S., 2004, PL-LFI-OAT-TN-033

[AD-6] *Static Maps of Zodiacal Light Emission for the Planck Mission* Maris M., Burigana C., 2006 Oct. 7th, PL-LFI-OAT-TN-055 (number erroneously assigned to another report, to be renumbered)

[AD-7] *Attitude History File ICD* Tuttlebee, M.,J. 2009 July 24th, Issue 2.6 or higher, DMS Document ID : PT-PMOC-FD-ICD-2110-OPS-GFT; PTGS Document ID: PGS-ICD-006

Reference Documents

[RD-1] Kelsall, T., Weiland, J.T., Franz, B.A., Reach, W.T., Arendt, R.G., et al., 1998, ApJ, 508, 44 (also astro-ph/9806250)

[RD-2] Fixsen, D.J., & Dwek, E., 2002, Ap.J., 578, 1009

[RD-3] Wheelock, S.L., Gautier, T.N., Chillemi, J., Kester, D., McCallon, H., et al., 1994, IRAS Sky Survey Atlas Explanatory Supplement, JPL Pubbl. 94-11

[RD-4] Maris, M., Burigana, C., Fogliani, S., 2005, *Zodiacal Light Emission in the* PLANCK *mission*, A&A, 2006, 452, 685-700.

[RD-5] The `JPL-Horizons` service and its documentation is availlable at the site `http://ssd.jpl.nasa.gov/?horizons`

2 Scope of the document

This report is a followup of [AD-1] [AD-3] [AD-4] [AD-5] and [AD-6] describing the maps of *Zodiacal Light Emission* (ZLE) generated for use in the PLANCK simulated mission. It describes maps generated for the first 492 days of mission.

This report superseeds the old [AD-1] [AD-3] [AD-4] [AD-5] [AD-6].

2.1 Limits of Applicability

In the current issue 2011 Jan 29$^{\text{th}}$, 0.1 the document refers to the Demonstrative Maps for Boresight Angle, $\beta = 85°$ and Frequency 857 GHz and for ODs between 91 and 582, released as a test of the simulation code `ZOD_F90` before its final release to the Level-S.

3 Introduction

The *Zodiacal Light Emission* (ZLE) due to thermal emission from the Interplanetary Dust Particles (IDPs) is the far-infrared (Far-IR) counterpart of the familiar Zodiacal Light due to scattering of the solar light by IDPs. Our starting point to reconstruct the spatial distribution of the ZLE, is the model of [RD-1] for the ZLE based on the COBE data (hereafter indicated as *COBE-model*) has many similarities with the IRAS model by [RD-3]. It describes in details the emissivity of the IDPs cloud, assumed to extend up to $\simeq 5.2$ AU far from the Sun, for wavelengths up to about 300 μm. According to the COBE-model four components contribute to the ZLE

1. the dominating *Smooth component*,
2. three *Bands of dust*,
3. an *Earth orbit locked ring* of dust (or *Circumsolar ring*),
4. the *Trailing blob*,

With respect to other foregrounds usually considered in CMB studies, the ZLE (as the other Solar System objects) is peculiar, depending its flux not only on the pointing direction but also on the instantaneous position of the observer and of the Sun within the Solar System leading to a well defined time dependence.

The flux calculated for a given feed-horn of a frequency band is

$$F_{ZLE,f}(\widehat{\mathbf{P}}(t),\mathbf{R}_\odot(t),\mathbf{R}_\mathrm{P}(t)) = \sum_{i_\mathrm{component}=\{1,21,22,23,41,42\}} F_{i_\mathrm{component},f}(\widehat{\mathbf{P}}(t),\mathbf{R}_\odot(t),\mathbf{R}_\mathrm{P}(t)). \quad (1)$$

Here $F_{ZLE,f}$ is the flux of ZLE for a feed-horn of frequency f, the index $i_\mathrm{component}$ denotes the specific ZLE component either the *Smooth component* ($i_\mathrm{component}=1$) [1], one of the three *Bands of dust* ($i_\mathrm{component}=21$, 22, 23 respectivelly), the *Earth orbit locked ring* of dust ($i_\mathrm{component}=41$), and the Earth *Trailing blob* ($i_\mathrm{component}=42$), $\mathbf{R}_\odot$ and $\mathbf{R}_\mathrm{P}$ denotes respectivelly the positions of the Sun and of the observer within the Solar System at the epoch t of the observation, while $\widehat{\mathbf{P}}$ the direction toward which the feed-horn for which the map is geneated is directed. Vectors $\mathbf{R}_\odot$, $\mathbf{R}_\mathrm{P}$ and $\widehat{\mathbf{P}}$ are defined by using J2000 Ecliptical Reference Frame, centered on the Solar System Baricenter (SSB).

Since IDPs does not radiate as Black Bodies, and since their effective Far-IR emissivity ϵ_f is not well constrained the $F_{i_\mathrm{component},f}$ is defined as

$$F_{i_\mathrm{component},f}(\widehat{\mathbf{P}}(t),\mathbf{R}_\odot(t),\mathbf{R}_\mathrm{P}(t)) = E_{i_\mathrm{component},f} Z_{i_\mathrm{component},f}(\widehat{\mathbf{P}}(t),\mathbf{R}_\odot(t),\mathbf{R}_\mathrm{P}(t)), \quad (2)$$

where $E_{i_\mathrm{component},f}$ is a largely (50%) uncertain emissivity correction (see App. B) and $Z_{i_\mathrm{component},f}$ is the brightness integral along $\widehat{\mathbf{P}}$

$$Z_{i_\mathrm{component},f}(\mathbf{P},\mathbf{R}_\odot,\mathbf{R}_{\widehat{\mathbf{P}}}) = \int_0^{s_\mathrm{max}} n_{i_\mathrm{component}}(\mathbf{r}(s)) B_f(T(R_\mathrm{Helio}(s)))ds, \quad (3)$$

with s the distance from the spacecraft ranging from 0 to s_max which is defined by the upper limit of 5.2 AU for the heliocentric distance $R_\mathrm{Helio}(s) = \left|\mathbf{R}_\mathrm{P} + s\widehat{\mathbf{P}} - \mathbf{R}_\odot\right|$. Also $\mathbf{r}(s) = \mathbf{R}_\mathrm{P} + s\widehat{\mathbf{P}}$, while

[1] We used here the $i_\mathrm{component}$ convention of the `ZOD_F90` simulator [AD-2].

Scan	ODs Range			ODs
1	91	-	260	152
2	261	-	430	170
3	431	-	582	170

Table 1: Definition of subscans.

$T(\mathbf{r}(s))$ is the temperature of an IDP grain at distance s from the spacecraft. In this respect the model assumes:

$$T(R_{\rm Helio}) = \frac{T_0}{R^{\delta}_{\rm Helio}}. \tag{4}$$

The most probable value of δ ($= 0.467$) is very close to the theoretical value of 0.5 for large grey grains in radiative equilibrium, while $T_0 = 286$ K.

4 Generation of Maps

Maps for each component are generated assuming $E_f = 1$. After that proper Ef scaling is applied as a second step and then component maps are summed together.

Maps presented in Sect. 5 are generated for ODs between 91 and 582. To analyze seasonal variability and time dependences the interval of ODs considered is splitted in three sub scans as detailed in Tab. 1 in App. A. The map for the complete set of scans can be easily recovered from these subscans see App. D.

From Eq. 1 it is evident as the $F_{{\rm ZLE},f}$ for a given direction in the sky, as an example the direction defined by a pixel in a `HEALPix` map, is a function of the epoch of observation t through $\mathbf{R}_{\rm P}(t)$ and $\mathbf{R}_{\odot}(t)$. The map–making procedure computes the average of TOD samples entering a given pixel $i_{\rm pix}$ taken at different times, so it averages over a discrete list of $F_{{\rm ZLE},f}(t)$ values. Having to deal with a complex scanning strategy, the best way to generate a ZLE map from Eq. 1 is to simulate the averaging procedure, this means to model

1. Map–making procedure.
2. Scanning strategy, giving
   $$\widehat{\mathbf{P}}_{t_{\rm smp}} = \widehat{\mathbf{P}}(t = t_{\rm smp});$$
3. Planck and Sun motions giving
   $$\mathbf{R}_{{\rm P},t_{\rm smp}} = \mathbf{R}_{\rm P}(t = t_{\rm smp}),$$
   and
   $$\mathbf{R}_{\odot,t_{\rm smp}} = \mathbf{R}_{\odot}(t = t_{\rm smp}).$$

where $t_{\rm smp}$ is the time at which a given sample in a TOD was acquired.

In this regard, map–making is modelled as a form of coadding of samples taken within a TOD i.e. for each frequency and each component

$$Z_{f,i_{\rm component},i_{\rm pix}} = \frac{\sum_{t_{\rm smp}\in\mathcal{H}_{i_{\rm pix}}} Z_{f,i_{\rm component},t_{\rm smp}}}{N_{{\rm hits},i_{\rm pix}}} \tag{5}$$

where $\mathcal{H}_{i_{\rm pix}}$ is the list of samples entering the pixel $i_{\rm pix}$, $N_{{\rm hits},i_{\rm pix}} \geq 0$ is the number of elements in $\mathcal{H}_{i_{\rm pix}}$, $Z_{f,i_{\rm component},t_{\rm smp}}$ is the contribution of the given ZLE component calculated for $\widehat{\mathbf{P}}_{t_{\rm smp}}$, $\mathbf{R}_{{\rm P},t_{\rm smp}}$ and $\mathbf{R}_{\odot,t_{\rm smp}}$. For the `HEALPix` pixelization scheme used here $\mathcal{H}_{i_{\rm pix}}$ is defined by using the `VEC2PIX_xxxx` or `ANG2PIX_xxxx` functions associating at a given $\widehat{\mathbf{P}}$ the appropriated $i_{\rm pix}$.

The $\mathbf{R}_{\odot,t_{\rm smp}}$ and $\mathbf{R}_{{\rm P},t_{\rm smp}}$ are interpolated at times $t_{\rm smp}$ from tables of $\mathbf{R}_{\odot}(t)$ and $\mathbf{R}_{\rm P}(t)$ generated by the `JPL-Horizons` service [RD-5]. Tables are sampled once every 15 min and are updated at the latest version of the effective PLANCK orbit [2].

The reconstruction of pointings is a cumbersome task given the large amount of data taken by PLANCK over a single pointing period. On the other hand, for a moderated resolution map (e.g. a map with $N_{\rm side} \leq 512$) lots of samples enters the same pixel, sampling within few arcmins the same region of sky and being acquired within one hour. Since the $\mathbf{R}_{\odot}(t)$ and $\mathbf{R}_{\rm P}(t)$ does not change in a sensitive manner over such a short period of time, and since ZLE changes over a typical angular scale of several degrees, it is possible to assume $\mathbf{R}_{\odot}(t)$ and $\mathbf{R}_{\rm P}(t)$ as constant over a pointing period, and $Z_{f,i_{\rm component}}$ to be constant over a single pixel.

The list of map pixels scanned by a given PLANCK feed–horn can be readilly recovered from the time averaged direction of the PLANCK spin axis $\widehat{\bar{\mathbf{S}}}$ during the stable pointing intervall of the given pointing period provided by the PLANCK *Attitude History File* (AHF) [AD-7]. Assuming the feed–horn looks in the sky at fixed separation from the PLANCK spin axis given by its effective boresight angle

$$\beta_{\rm eff,fh} = \arccos \widehat{\mathbf{P}}_{\rm fh} \cdot \widehat{\bar{\mathbf{S}}}, \tag{6}$$

the relevant pixels in the map are those which intersects a ring centered on $\widehat{\bar{\mathbf{S}}}$ and angular radius $\beta_{\rm eff,fh}$ [3].

So the algorithm to generate the maps presented here is

1. Define a ZLE Map $\{Z_{i_{\rm pix}}, i_{\rm pix} = 0 \ldots 12{N_{\rm side}}^2 - 1\}$ and an hits map $\{H_{i_{\rm pix}}, i_{\rm pix} = 0 \ldots 12{N_{\rm side}}^2 - 1\}$, both of them filled with zeros.
2. Each pointing period in the required intervall of ODs (identified by its unique $i_{\rm spin}$ index [4]):
   (a) take $\widehat{\bar{\mathbf{S}}}_{i_{\rm spin}}$ and find the corresponding set of map pixels $\mathcal{S}_{i_{\rm spin}}$ visited by the corresponding scan circle;
   (b) increment by 1 the elements of the $\{H_{i_{\rm pix}}\}$ map in the $\mathcal{S}_{i_{\rm spin}}$;
   (c) interpolate $\mathbf{R}_{\odot}(t)$ and $\mathbf{R}_{\rm P}(t)$ at mid–time of the stable pointing period [5]

$$t_{\rm stable,mid} = \frac{1}{2}\left(t_{\rm stable,start} + t_{\rm stable,end}\right)$$

   (d) by using $\mathbf{R}_{\odot}(t_{\rm stable,mid})$ and $\mathbf{R}_{\rm P}(t_{\rm stable,mid})$ compute $Z_{f,i_{\rm component}}$ assuming as $\widehat{\mathbf{P}}$ the coordinates of the map pixels in the $\mathcal{S}_{i_{\rm spin}}$, and increment the values of the corresponding elements in the $\{Z_{i_{\rm pix}}\}$ map.

[2] As the mission proceeds ESA Flight Dynamics updates the on a regular basis the PLANCK orbit in the `JPL-Horizons` database, so that predictions are replaced by measured positions and velocities of the PLANCK spacecraft.

[3] Usually the scan circle is oversampled of at least a factor of ten with respect to the map resolution, repeated "hits" on the same pixel within a scan circle are susequently removed.

[4] Of course the poiting periods not used for scientific acquisition are skipped.

[5] The `AHF` gives the start and end times of each stable pointing period.

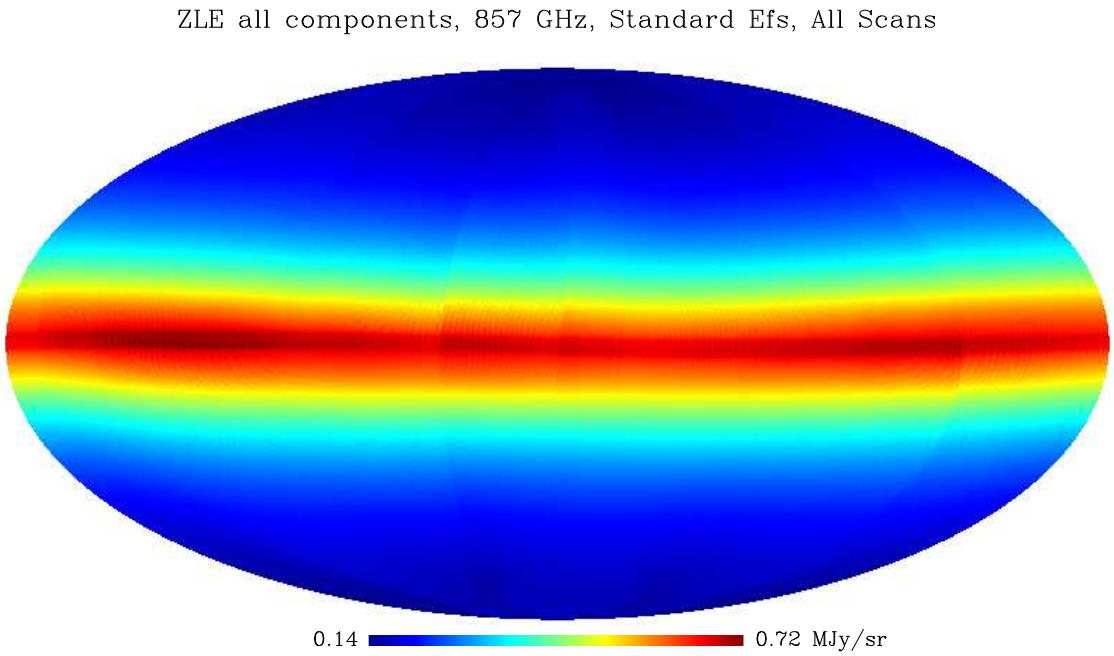

Figure 1: ZLE integrated over ODs 91 to 582, scans 1+2+3, all components. The figure is drawn in ecliptical coordinates and it is centered at ecliptical longitude 0° and latitude 0°. `FITS` file: `zle_all_fh0000_g857_ecl_nside512_all_scans.fits`

3. for each element of $\{Z_{i_{\rm pix}}\}$ for which $H_{i_{\rm pix}} \neq 0$ compute the ratio $Z_{i_{\rm pix}}/H_{i_{\rm pix}}$ (the other elements are filled with zeros or `NaN` values).

The time required on a single 2 GHz processor to perform such calculation for a time intervall of 412 ODs with $N_{\rm side} = 512$ is of about 3 hours. The averaged time elapsed for a single ring being about 3×10^{-2} sec. Since in its present version the simulator computes 5 different integrals for each pixel and each ZLE component (over the flux) it is possible to accelearate the calculation of a factor of 5 simply avoiding those extra calculations. More over since ODs are managed independently, it is very easy to parallelize the procedure described above on a multiprocessor machine, without the need to parallelize directly the `FORTRAN` ZLE code.

5 Maps

The scope of this report is to provided a dimostrative analysis of the expected pattern of ZLE contamination. As a consequence the simulation presented here refers to a representative feed–horn at 857 GHz with $\beta_{\rm eff,fh} = 85°$, more complete maps will be prepared with the collaboration of the Level–S team. We assumed in these maps "standard" E_f values as defined in App. B.

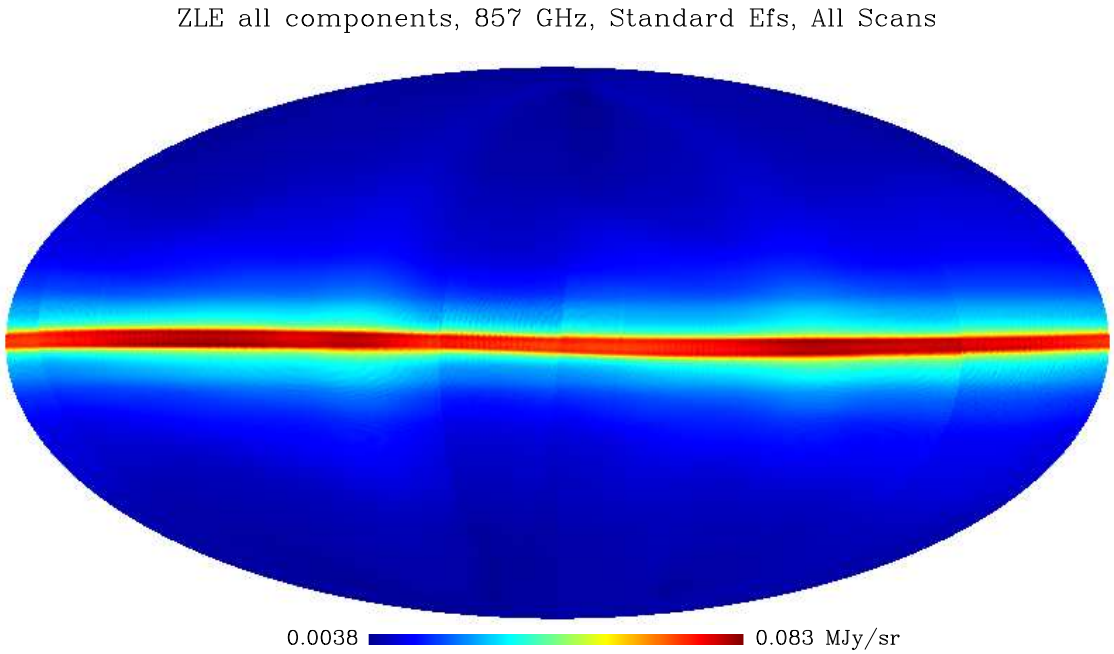

Figure 2: Contribution of secondary components integrated for all the scans.

Unless stated differently, in the following all the figures will be drawn in ecliptical coordinates and centered on ecliptical longitude 0° and ecliptical latitude 0°.

5.1 Predicted level of ZLE contamination

Fig.s 1, represents the ZLE map obtained by coadding all the simulated data for ODs 91 - 582. The peak ZLE contamination expected from this simulation maps is about 0.55 MJy/sr at 857 GHz However, as already discussed in [RD-4] the level of uncertainties in E_f estrapolation from COBE/-FIRAS data allows up to a factor of two larger contamination.

> **To asses proper removal of ZLE contamination an independent measure of E_f based on PLANCK data must be accomplished.**

It is also evident the presence of strange features on the map, which are more evident when maps for the three individual subscans defined in App. A are produced. Since templates for these subscans are released as `FITS` files, those maps are presented in Fig.s 3, 4 and 5, while their analysis is reported in Sect. 5.3.

5.2 Secondary Components

Fig. 2 represents the contribution of all of the secondary components to Scan 1. Most of the contribution is concentrated around the ecliptical plane, and it is due to the effect of the Bands. With the standard E_f used here secondaries contributes to the total ZLE contamination for at most $\approx 16\%$. Those figures are in line with those reported in Tab. 3 computed for the 2006 issue of the maps.

Given the limited contribution of those components to the ZLE contamination, in most of the subsequent analysis we will considered just the dominat Smooth component. A more complete analysis is in preparation.

5.3 Discontinuities

The most relevant feature on the map is the presence of evident discotinuities in the ZLE distribution. As an example following in Fig.s 3 the ZLE along the line of peak emissivity, located at some degree around the ecliptic, it is evident the presence of two maxima. with a clear discontinuty at the left side of the map, near its center. Similar patterns occurs in Fig. 4 and Fig. 5. The peak–to–peak variation of the maximal flux across the discontinuities border is about 20%.

Such discontinuities, already analyzed in [AD-6], are due to the combination of the about half–year periodicity of the scanning strategy with the about yearly periodicity of $\mathbf{R}_\odot(t)$ and $\mathbf{R}_\mathrm{P}(t)$. They can not be considered as an artefact of the integration method and they vanishes increasing the length of the scan. This is clearly shown in Fig. 1 where all the samples from OD 91 up to OD 592 are integrated.

In particular, in the current scanning strategy the spin axis slowly precesses following a circle of about 7.5° around the *antisolar direction* (the Sun–PLANCK direction), so that for some time the spin axis preceeds the antisolar direction and for some other time it follows the antisolar direction in its orbit about the Sun.

We test the correctness of such interpretation by looking at a set of simplified cases in which which just the Smooth component is present, the Sun is located in the SSB and it does not moves, and PLANCK follows a circular orbit of 1.01 AU about an the Sun at a costant speed. In this model the Spin axis direction is shifted of a constant amount with respect to the antisolar direction and the sky is scanned by circles of $\beta_{\mathrm{eff,fh}} = 85°$. We considered five cases, in the first no shift is

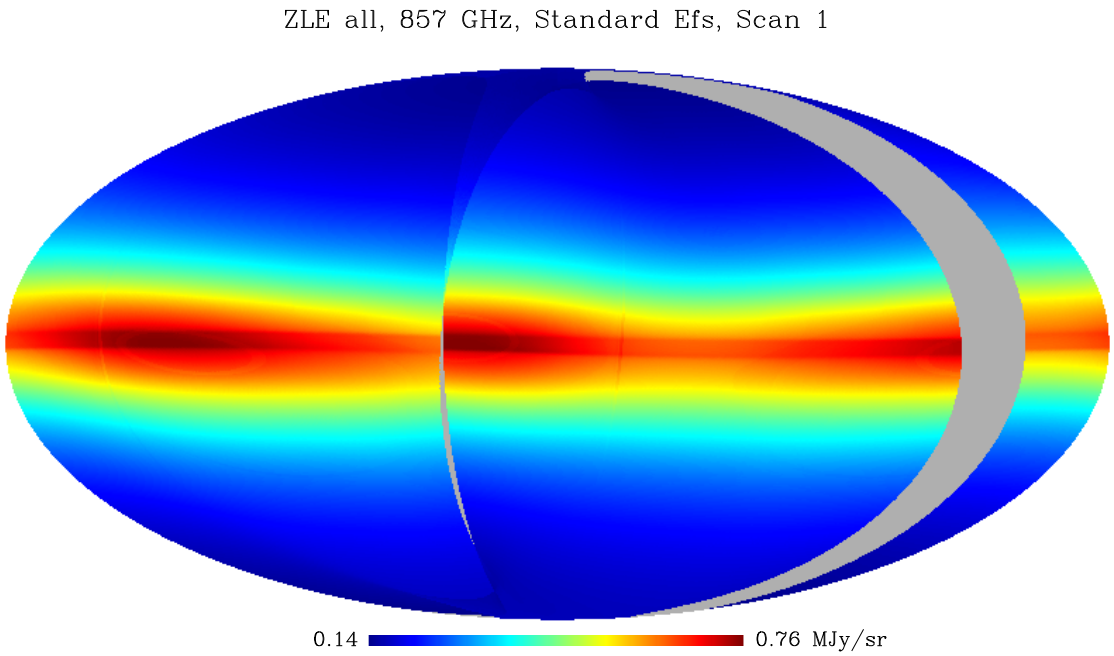

Figure 3: ZLE for Scan 1, OD 91 - 260, 152 ODs, All components, Standard Efs, 857 GHz, $N_{\rm side} = 512$, $\beta = 85°$, ecliptical coordinates. `FITS` file: `zle_all_fh0000_g857_ecl_nside512_scan1.fits`

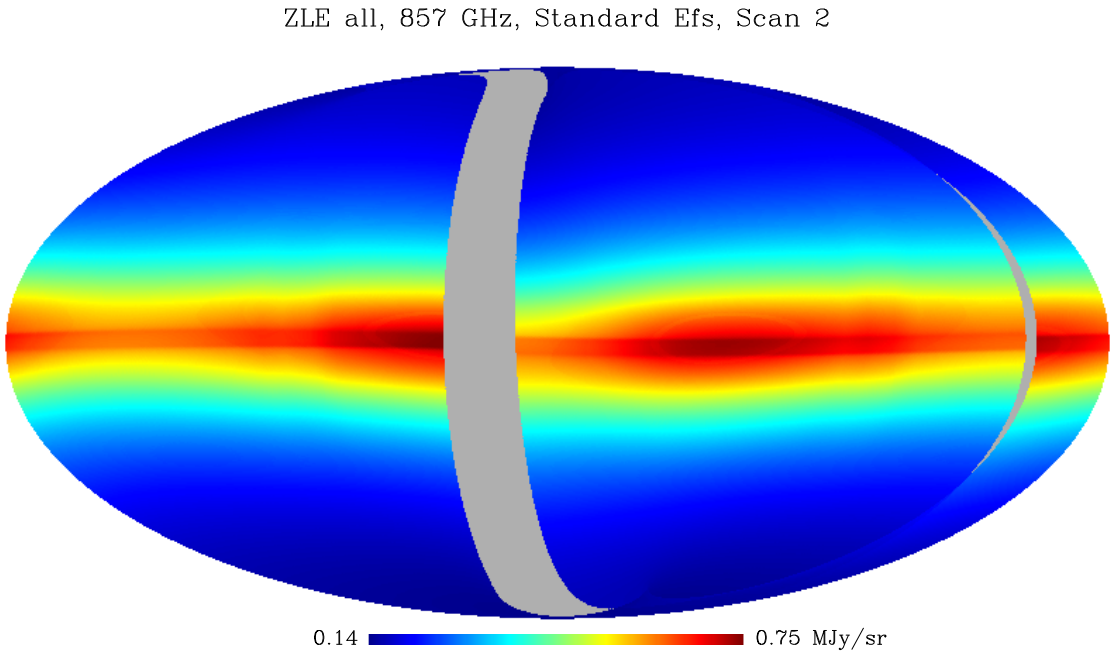

Figure 4: ZLE for Scan 2, OD 261 - 430, 170 ODs, All components, Standard Efs, 857 GHz, $N_{\rm side} = 512$, $\beta = 85^\circ$, `FITS` file: `zle_all_fh0000_g857_ecl_nside512_scan2.fits`

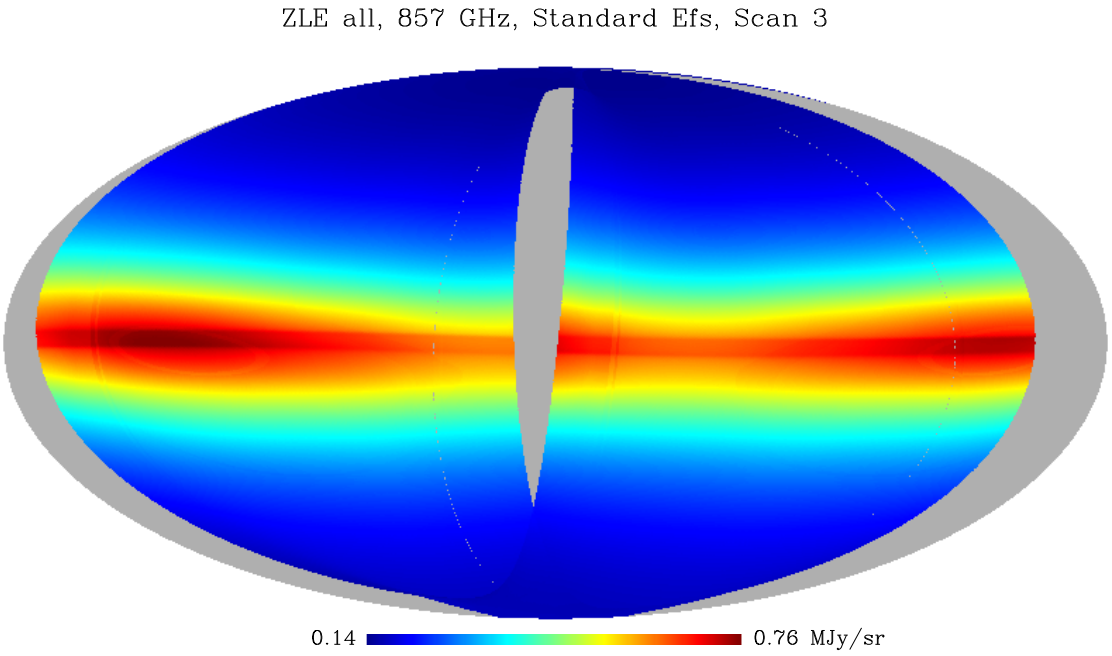

Figure 5: ZLE for Scan 3, ODs 431 - 582, 170 ODs, All components, Standard Efs, 857 GHz, $N_{\rm side} = 512$, $\beta = 85^\circ$, FITS file: `zle_all_fh0000_g857_ecl_nside512_scan2.fits`

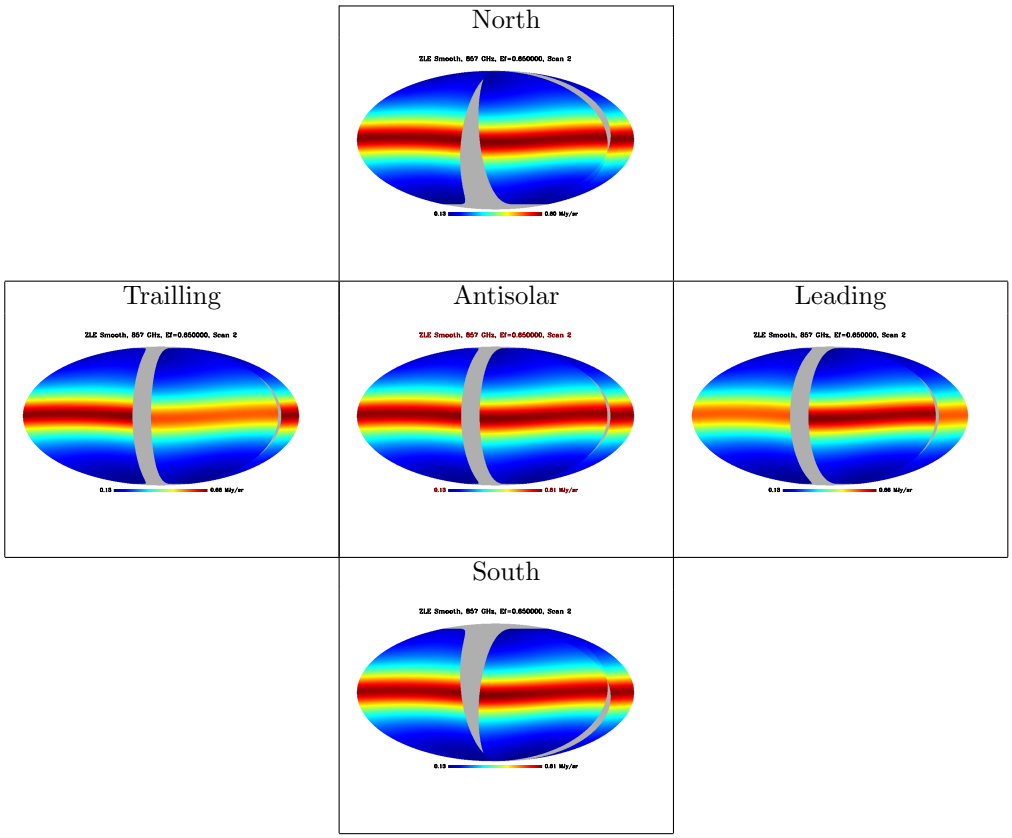

Figure 6: Simplified scanning of the Smooth ZLE component, for Scan 2. In the central frame the spin axis is kept aligned with the antisolar direction. In the left and right frames the spin axis is kept on the ecliptic but it is kept shifted in ecliptical longitude of -7.5° (trailling) or $+7.5^\circ$ (leading) with respect to the antisolar direction. Similarly in the upper (North) and lower (South) frames the ecliptical longitude of the spin axis is kept equal to the ecliptical longitude of the solar direction, but the spin axis is shifted of $\pm 7.5^\circ$ in latitude.

applied, in the second and in the third case the shift is applied just in longitude, while in the remaining cases the shift is applied just in latitude. To simplify the analysis we concentrate on Scan 2, the other scans giving similar results.

The result is shown in Fig. 6 the central frame is for null–shift, left and right frames are for shifts in longitude, upper and lower frames are for shifts in latitude. The central map is not completelly smooth, the reason is that in this model we did not put at zero the tilt of the IDPs cloud and its shift with respect to the Sun. However it is evident how moving along the equator most of the discontinuities of Fig. 4 are no longer present. Looking at the Trailling frame it is evident how the ZLE is enhanced on the Trailling side of the map and it is depressed on the leading side. The opposite pattern occurs in the Leading frame. The difference is smaller for the North and the South.

The largest differences of the Leading - Trailling and of the North - South maps are shown in the top row of Fig. 7. For the Leading-Trailling the largest effect amounts at ± 0.08 MJy/sr, equivalent at $\approx 16\%$ of the Smooth component contribution, while for North - South the effect is ± 0.02 MJy/sr or $\approx 4\%$.

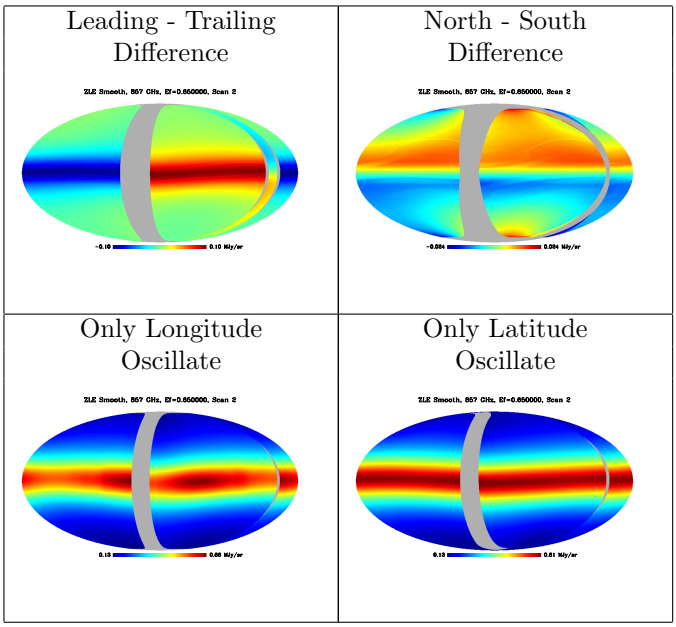

Figure 7: Top the difference between leading - trailing and North - South maps for Scan 2. Bottom the effect of limiting the oscillation of the Spin axis along the longitude (at left) and the latitude (at right).

This implies that the largest effect of the spin axis precession is connected to its changes in longitude, as shown by the lower part of Fig. 7 where maps for Scan 2 are produced assuming the same scanning strategy of PLANCK but at left leaving just the longitude to vary and the right leaving just the latitude to change. It is evident how the case in which just the longitude changes resembles very well the pattern shown by Scan 2 map in Fig. 4.

It is easy to understand the reason of such effect. The ZLE distribution has a minimum when looking toward the antisolar direction, and increases more or less parabolically on the ecliptical plane decreasing the solar elongation. Scan circles drawn with spin axis centered on the antisolar direction cuts the ecliptical plane at the same solar elongation, and are consequently longitudinally symmetrical. A scan circle drawn from a shifted spin axis will have a side which will cross the ecliptic equator more near to the antisolar direction than in no–shift case so it will see a smaller signal in that case. The opposite will occur for the other side which will detect a larger signal. The amount of variation at the peak signal with the longitudinal shift $\Delta\lambda$ is about at $\beta_{\rm eff,fh} = 85°$

$$F_{\rm ZLE,857GHz,peak} \approx E_{\rm 857GHz}(0.936 + 0.0102\Delta\lambda)\,{\rm MJy/sr}. \quad (7)$$

So an oscillation in attitude leading to a $\Delta\lambda$ of $\pm 7.5°$ will produce a $\pm 8.1\%$ variation in the peak ZLE signal.

Apparent discontinuities will appear if a map is obtained assembling rings which are taken while the spin axis is leading and rings taken with trailing spin axis.

5.4 Seasonal modulation

In [RD-4] it have been discussed the possibility to separate the ZLE from the background by looking at its *seasonal modulation* due to the differences in $\mathbf{R}_\odot$ and $\mathbf{R}_{\rm P}$ when taking data in

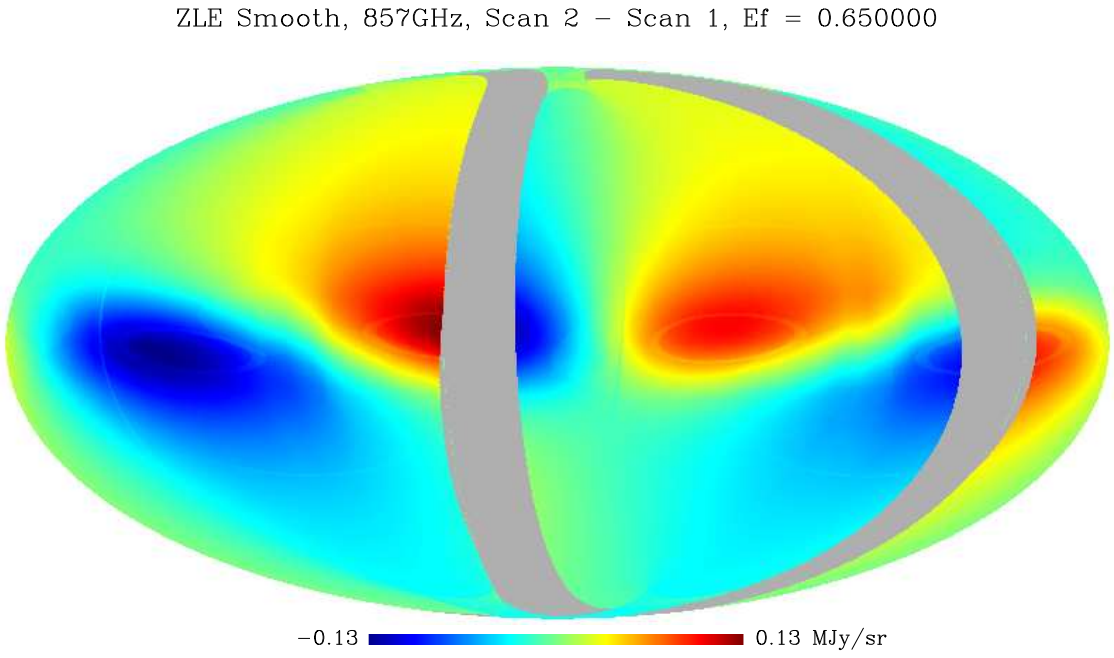

Figure 8: Seasonal modulation, difference between Scan 2 and Scan 1, smooth component only.

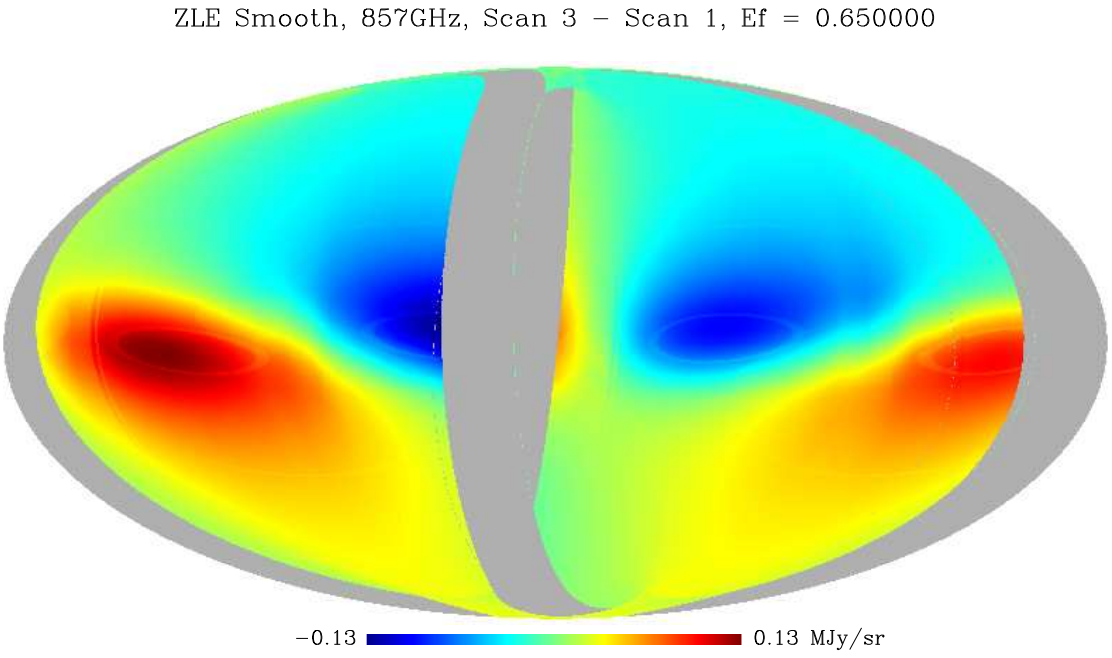

Figure 9: Seasonal modulation, difference between Scan 3 and Scan 2, smooth component only.

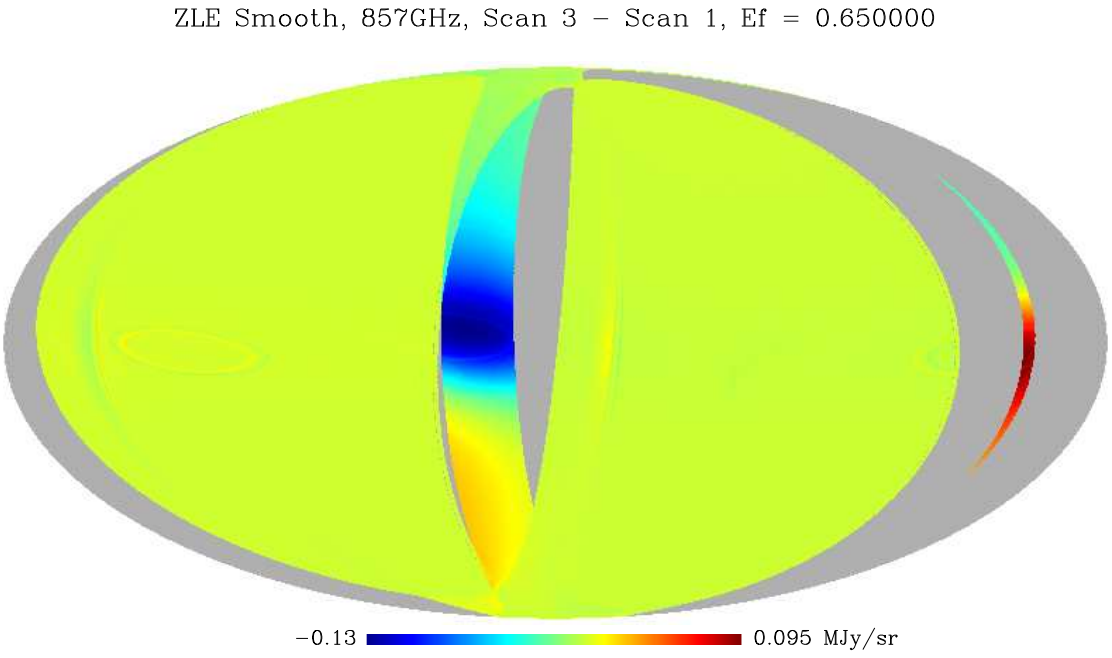

Figure 10: Seasonal modulation, difference between Scan 3 and Scan 1, smooth component only.

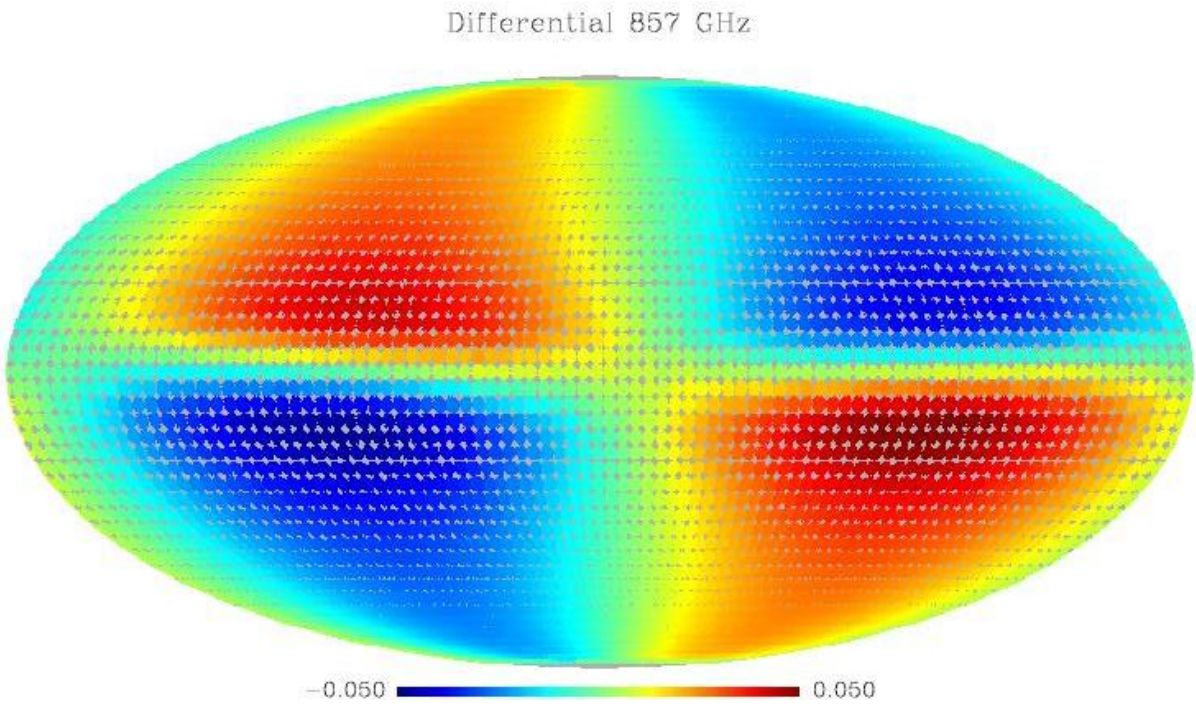

Figure 11: Prediction of seasonal modulation between two subsequent scans for the old (2006) baseline for the Scanning Strategy. The map is splitted in round patches of 2° radius due to the calculation method used at that epoch.

subsequent scans of the same region of sky. Seasonal modulation combines with the changes in the angular distances of the antisolar direction of the spin axis. In its simplest version, if $I(\widehat{\mathbf{P}}, t_{\rm scan})$ represents the flux measured toward a given direction of sky at the epoch of a scan $t_{\rm scan}$ it could be decomposed into ZLE and Background contribution

$$I(\widehat{\mathbf{P}}, t_{\rm scan}) = F_{\rm ZLE}(\widehat{\mathbf{P}}, \mathbf{R}_{\odot}(t_{\rm scan}), \mathbf{R}_{\rm P}(t_{\rm scan})) + F_{\rm Background}(\widehat{\mathbf{P}}), \tag{8}$$

in the ideal case in which $\widehat{\mathbf{P}}$ are perfectly repeated between two scans $t_{\rm scan,1}$ and $t_{\rm scan,2}$

$$\Delta I(\widehat{\mathbf{P}}) = F_{\rm ZLE}(\widehat{\mathbf{P}}, \mathbf{R}_{\odot}(t_{\rm scan,2}), \mathbf{R}_{\rm P}(t_{\rm scan,2})) - F_{\rm ZLE}(\widehat{\mathbf{P}}, \mathbf{R}_{\odot}(t_{\rm scan,1}), \mathbf{R}_{\rm P}(t_{\rm scan,1})). \tag{9}$$

Which shows that in principle the analysis of the seasonal modulation would allow a self–consistent measure of the various ZLE parameters, since it would allow a complete removal of the background.

A full simulation of the seasonal modulation is outside the scope of this report, but a simplified method of analysis is to look at the difference of maps of subsequent subscans. Fig. 8 represents the pattern of differences between Scan 2 and Scan 1 for the Smooth component only. A pattern composed of 4 spots located around the ecliptic plane is evident. Spots of positive and negative variation are more or less simmetrically distributed, with a peak–to–peak variation of ≈ 0.18 MJy/sr, equivalent at a peak–to–peak $\approx 40\%$ modulation. The pattern is modulated by the effect of the scanning strategy as shown by looking at Fig. 11 which is the previous simulated seasonal modulation as expected for the old (2006) baseline for the Planck scanning strategy, it is evident how a smooth quadrupolar pattern arises with the peak differences occurring near

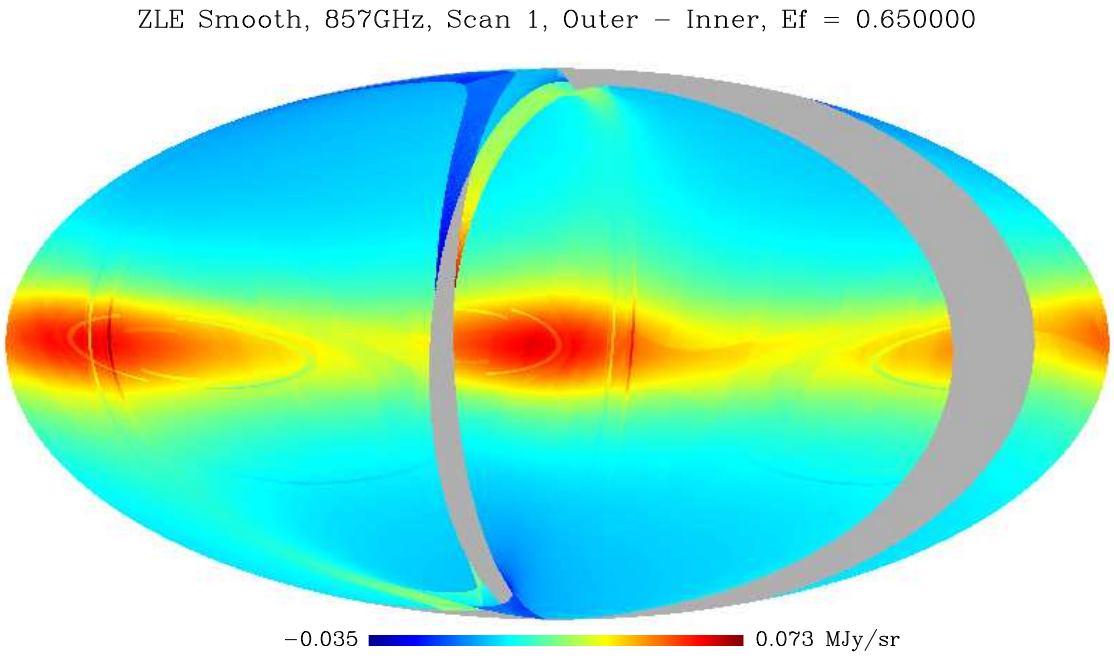

Figure 12: Peak–to–peak changes in the ZLE Smooth component for moving $\beta_{\rm eff,fh}$ across the Focal Plane, i.e. from 88.7614° (outer) to 82.4299° (inner).

the ecliptic. Fig. 9 shows the difference between Scan 3 and Scan 2 the same pattern arises but with reversed signs, indicating that Scan 3 and Scan 1 largely overlap as shown by Fig. 10. This allows to conclude that it will be possible to enhance the seasonal dependence by coadding maps of differences between Scan 4 and Scan 3 and Scan 2 and Scan 1.

5.5 Changes in Boresight Angle

All the simulations presented here are for a fixed $\beta_{\rm eff,fh} = 85°$, however the PLANCK focal plane is few degrees wide, so that different feed horns sees slighlty different ZLE contamination patterns. Fig. 12 shows the difference in the Smooth component pattern variing $\beta_{\rm eff,fh}$ across the Focal Plane, i.e. from 88.7614° (outer) to 82.4299° (inner). It is evident how the largest differences are in the longitudinal distribution and amount at a maximum change of 0.07 MJy/sr, less than 10% of the total ZLE contamination. Similar changes occurs for the other two scans and for the three scans coadded map.

A Subscans definition

Tab. 1 defines the three subscans used in this report. The main aim of the subscan definition is to allow the creation of maps of ZLE derived from TOD samples which are as more as possible homogeneous in $\mathbf{R}_{\odot}(t)$ and $\mathbf{R}_{\mathrm{P}}(t)$, avoiding to coadd in the same map samples acquired in times too much different, with long intervalls of time in which the pixel is not scanned.

The level of time contiguity in samples entering each pixel depends on the ecliptical latitude. While near the equator observation occurs in "bursts" of few days every many weeks, at the poles pixels are nearly continuously observed. Since the scope of subscans definition is to evidence relevant seasonal dependences at low ecliptical latitudes, where the ZLE has its maximal power, the subscans are defined as the longest intervalls of contiguous ODs with minimall or null overlap at ecliptical latitudes between -45° and +45° and maximal coverage of the map.

f [GHz]	$\langle I_{\nu=f}\rangle^{\rm FD}_{\rm year}$ [MJy/sr]	$\langle Z_f\rangle_{\rm year}$ [MJy/sr]	$E_f^{\rm FD}$
30	0.0000	0.0006	0.001
44	0.0000	0.0013	0.002
70	0.0000	0.0032	0.004
100	0.0001	0.0064	0.009
143	0.0002	0.0129	0.018
217	0.0012	0.0291	0.041
354	0.0083	0.0755	0.110
545	0.0458	0.1751	0.262
857	0.2742	0.4229	0.648

Table 2: $E^{\rm FD}_{f,\rm Smooth}$ estimated according to Eq. (10).

	Expected Peak Fluxes [Jy/sterad]						
Freq.	Smooth		Trailing	Locked			
[GHz]	Component	Band 2	Blob	Ring	Band 1	Band 3	Total
30	2.1×10^{2}	7.3×10^{1}	5.7×10^{1}	3.3×10^{1}	1.2×10^{0}	$1.5\times10^{-}1$	3.6×10^{2}
44	5.1×10^{2}	1.6×10^{2}	1.2×10^{2}	7.1×10^{1}	2.5×10^{0}	$3.2\times10^{-}1$	8.2×10^{2}
70	1.5×10^{3}	4.0×10^{2}	3.1×10^{2}	1.8×10^{2}	6.3×10^{0}	$8.1\times10^{-}1$	2.3×10^{3}
100	3.4×10^{3}	8.1×10^{2}	6.3×10^{2}	3.7×10^{2}	1.3×10^{1}	1.7×10^{0}	5.0×10^{3}
143	7.6×10^{3}	1.6×10^{3}	1.3×10^{3}	7.5×10^{2}	2.6×10^{1}	3.4×10^{0}	1.1×10^{4}
217	2.0×10^{4}	3.8×10^{3}	2.9×10^{3}	1.7×10^{3}	5.9×10^{1}	7.7×10^{0}	2.7×10^{4}
353	5.9×10^{4}	9.8×10^{3}	7.6×10^{3}	4.5×10^{3}	1.5×10^{2}	2.0×10^{1}	7.9×10^{4}
545	1.6×10^{5}	2.3×10^{4}	1.8×10^{4}	1.0×10^{4}	3.6×10^{2}	4.6×10^{1}	2.0×10^{5}
857	4.3×10^{5}	5.4×10^{4}	4.3×10^{4}	2.5×10^{4}	8.5×10^{2}	1.1×10^{2}	5.4×10^{5}

Table 3: Expected peak fluxes for the ZLE components at different Planck frequencies.

B Tables of E_f

As already discussed in [RD-4] a frequency dependent, emissivity correction factor $E_f < 1$ has to be applied to the ZLE maps in order to obtain the final brightness. There are various options in estimating E_f, but a convenient approximation for the Smooth component is approximated by [RD-4]

$$E^{\rm FD}_{f,\ \rm Smooth} \simeq 126.63 \left(\frac{f}{1.2\times10^{4}\rm GHz}\right)^{2}, \tag{10}$$

tabulated values are in Tab. 2.

So we take at 857 GHz an $E_f = 0.65$ for the Smooth component. For the other components it is difficult to draw a firm frequency dependence from COBE/DIRBE data, which shows a smaller variation than E_f for the Smooth component. Since those are demonstrative maps, we assume here for the secondary components $E_f \equiv 0.95$ and we left to a subsequent deepeer analysis the use of a more precise value of E_f for such components.

Tabulated peak fluxes for the various components are in Tab. 3

Column	Format	Name	Description
1	Flux [MJy/sr]	double	the computed flux in the pixel
2	Hits	long	number of simulated hits in the pixel (Note those are not the hits of a real map.)

Table 4: Table of `FITS` files columns.

Keyword	Format	Description
`Ef`	double	The Ef factor for the component in the map
	... Other keywords to be inserted ...	

Table 5: Table of `FITS` files keywords. Note all the keyword names begin with `HIERARCH`.

C `FITS` files format

`FITS` files are written in a two-columns `HEALPix` format by using the `WRITE_FITS_SB` procedure.

Maps have: Ring Ordering, $N_{\rm side} = 512$, Coordsys=Ecliptical J2000.

Pixels of maps not visited by the scanning strategy are filled with `NaN` values as defined by `IDL` "`!VALUES.D_NAN`" value.

Columns are described in Tab. 4.

Keywords are described in Tab. 5.

D Subscans Coadding

The procedure to coadd individual sub scan maps is:

1. define a `FLUX` map with all values 0
2. define a `HITS` map with all values 0
3. for each map-file :
   (a) Take column 1 of the file put in `F_FLUX`
   (b) Take column 2 of the file put in `F_HITS`
   (c) find all the pixels in the `F_HITS` with value 0 (if any)
   and replace with 0. their `F_FLUX` value
   (d) `FLUX=FLUX+F_FLUX*DOUBLE(F_HITS)`
   (e) `HITS=HITS+F_HITS`
4. for all the pixels for which `HITS`$\neq 0$
   `FLUX=FLUX/DOUBLE(HITS)`

the FLUX map contains the coadded map.
If wanted fill the pixels with `HITS`==0 (if any) with `NaN`.